J. Fluid Mech. (2001), *vol.* 430, *pp.* 1–26. Printed in the United Kingdom

Transport and mixing in Stokes flow: the effect of chaotic dynamics on the blinking stokeslet

By S. R. OTTO, A. N. YANNACOPOULOS AND J. R. BLAKE

School of Mathematics and Statistics, The University of Birmingham, Edgbaston, Birmingham, B15 2TT, UK

(Received 26 January 1999 and in revised form 14 August 2000)

Mixing and transport processes associated with slow viscous flows are studied in the context of a blinking stokeslet above a plane rigid boundary. Whilst the motivation for this study comes from feeding currents due to cilia or flagella in sessile micro-organisms, other applications in physiological fluid mechanics where eddying motions occur include the enhanced mixing which may arise in 'bolus' flow between red blood cells, peristaltic motion and airflow in alveoli. There will also be further applications to micro-engineering flows at micron lengthscales. This study is therefore of generic interest because it analyses the opportunities for enhanced transport and mixing in a Stokes flow environment in which one or more eddies are a central feature.

The central premise in this study is that the flow induced by the beating of microscopic flagella or cilia can be modelled by point forces. The resulting system is mimicked by using an implicit map, the introduction of which greatly aids the study of the system's dynamics. In an earlier study, Blake & Otto (1996), it was noticed that the blinking stokeslet system can have a chaotic structure. Poincaré sections and local Lyapunov exponents are used here to explore the structure of the system and to give quantitative descriptions of mixing; calculations of the barriers to diffusion are also presented. Comparisons are made between the results of these approaches. We consider the trajectories of tracer particles whose density may differ from the ambient fluid; this implies that the motion of the particles is influenced by inertia. The smoothing effect of molecular diffusion can be incorporated via the direct solution of an advection–diffusion equation or equivalently the inclusion of white noise in the map. The enhancement to mixing, and the consequent ramifications for filter feeding due to chaotic advection are demonstrated.

1. Introduction

Many flows of biological and industrial importance can be characterized by having low Reynolds numbers. In many of these flows it is crucial to be able to ascertain levels of mixing and particle transport in such a viscous environment where inertial effects are totally unimportant. An excellent account of the rôle of mixing is given in Ottino (1989). Recently Hackborn, Ulucakli & Yuster (1997) have considered the structure of hyperbolic and degenerate mixing regions in Stokes flow; comparisons were made between theoretical and experimental findings. A phenomenon, which they dubbed Mel'nikov resonance, was identified, which is associated with lobe dynamics; Jana, Metcalfe & Ottino (1994).

In sessile organisms, such as *Vorticella* and *Stentor*, rings of cilia drive circulatory currents (Sleigh 1973). A class of micro-organisms, *choanoflagellates*, are characterized by having a collar and a flagellum; the helical motion of the flagellum generates a toroidal eddy. In Pettitt (2000) flows in the neighbourhood of one such micro-organism, namely *Salpingoeca Amphoridium*, are studied. In this experimental study the micro-organism relies on the ability to filter particles out of the fluid rather than moving to a fresh food source. By following the motion of small polystyrene spheres, their capture on the collar and subsequent ingestion is described and recorded. In order to model the far-field flow generated by the beating of the flagellum we assume that it can be mimicked using a point force, Blake & Otto (1996). To determine the flow field arising due to the stokeslet we solve the Stokes equations forced by a delta function multiplied by the force vector, this is affected by three-dimensional Fourier transforms. The presence of the solid boundary generates an image system which comprises an image point force (to satisfy the condition of no normal flow) a Stokes doublet and a source doublet (to satisfy the condition of no-slip), see figure 1. We refer the reader to Blake & Otto (1996) and the work of Lorentz (1896). If the point of application of these stokeslets remains stationary then flows with closed streamlines will be obtained and this will not lead to any degree of mixing (other than by molecular diffusion, which we assume to be relatively weak). However, if the location of the stokeslet changes a mechanism for enhanced mixing is dispersion induced by the corresponding chaotic advection. In Blake & Otto (1996) and Blake, Otto & Blake (1998) some preliminary discussion has been given, stating that flows comprising two point forces operating at different spatial points with distinct periods of operation can lead to chaotic particle paths, leading to enhanced mixing.

Stroboscopic plots of the flow were given which are akin to Poincaré sections. As the period of the system is increased, Blake & Otto (1996) found that the flow becomes 'more' chaotic, as also previously observed in the blinking vortex flow, Aref (1984). There, two point vortices were alternately switched on and off. If the switching is 'fast' it is as if both features are always turned on; however as the period of the system is increased, regions of local chaos occur close to the vortices. As the period is increased further there is a transition to global chaos. Another similar flow is the tendril-whorl flow (Khakhar, Rising & Ottino 1986). This flow is a combination of extensional flows and a twist map. The structures of period-1 and period-2 points are given, including a discussion of their nature. Mention is made of the homoclinic/heteroclinic structure and the resulting horseshoe dynamics. In this paper we exploit maps rather than flows, as this allows far greater analytical progress before recourse needs to be made to numerical calculations. The cost of the resulting calculations is also much reduced by the use of the map. The switching protocol is taken to be in the form of a periodic train of delta pulses. This allows us to construct a Poincaré or return map for the resulting flow. Unfortunately, in order to retain the area-preserving nature of the flow we are compelled to use an implicit map which increases the computational expense. This introduces a degree of uncertainty and we shall comment on the effect of this change and compare the results to those obtained via the direct solution of the full system. We exploit a map which deals with the inherent discontinuity by taking the mean of the left and right limits. Various island chain structures are identified, and as the time spent with each stokeslet (or equivalently its associated force) is increased these structures are eventually destroyed.

In biological problems one is often interested in the transport of particles whose properties may not be the same as the supporting media, for example in filter feeding

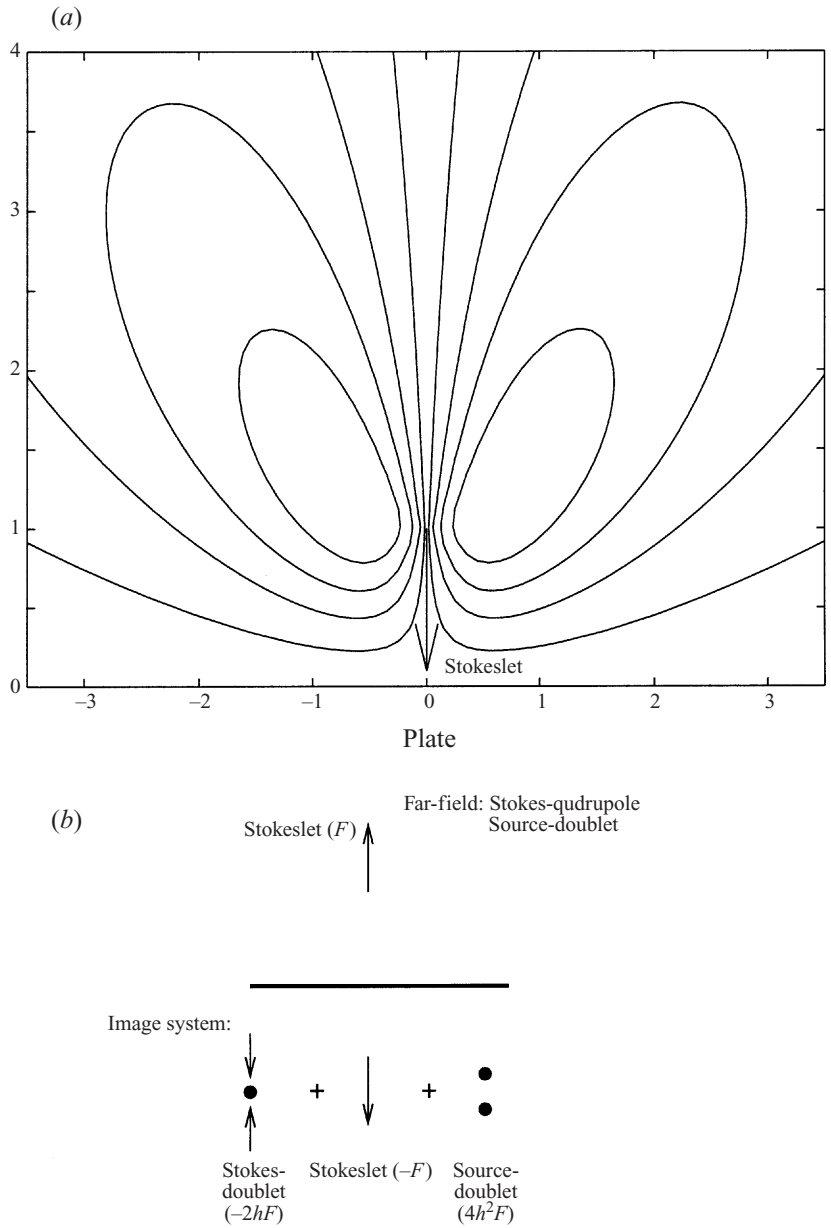

FIGURE 1. Streamfunction for a stokeslet situated at $(0, 1)$ above a plate (corresponding to $y = 0$). (*a*) Stream lines corresponding to a Stokeslet at $(0, 1)$. (*b*) Illustration of image system for a stokeslet near a rigid boundary.

of small particles in bivalve molluscs. In Maxey & Riley (1983) the transport of comparatively light and heavy spherical particles was discussed. In our problem this introduces a degree of inertia, and this means the particles will either be expelled from or trapped within the resulting eddies. A four-dimensional map is derived, and in the limit of large inertia response time a two-dimensional modification to the inertia-free map is found (Druzhinin & Ostrovsky 1994). In the current study we do not appear to find the strange attractors reported on in Omurtag, Dutta & Chevray

(1996) within bounded chaotic flows. We believe this is due to the unbounded nature of the flow herein, and its consequent similarity with chaotic scattering. In an attempt to quantify the amount of mixing present in the flow, we consider the effect on an element of fluid. A variety of measures are used for this purpose, and the basis for these techniques is to consider the Jacobian of the map. The long-time stretching of an element is measured in terms of Lyapunov exponents (LE). In this approach two particles are placed a small distance apart and their images are calculated. The extension (or contraction) of the distance between the point indicates the level of local dispersion. After successive iterations the distance between the points is renormalized, as the theory relies on the points being in close proximity. Calculations using this method will not necessarily determine which direction expands most; this is one problem which is overcome via the use of the map. Using the Jacobian (and its eigenvalues and eigenvectors) we can determine the local properties of the problem. The LE show regions from which fluid is likely to become well mixed. As noted in Ottino (1989) 'positive Lyapunov exponents imply an exponential rate of stretching of material elements, and hence, good mixing'. It is possible and indeed pertinent to use short-time or local Lyapunov exponents, which are described in due course.

Another technique which has been exploited is to construct the barriers to transport, Tang & Boozer (1996). It is noted in Tang & Boozer (1996) that the geometry of the stable foliation lines (s-lines) affects the diffusive transport via the local Lyapunov exponents (LLE). The variation of the LLE along the s-lines is instructive and Tang & Boozer note that local minima of the LLE occur at sharp bends in the lines. The construction of the s-lines is again related to the Jacobian of the map, although this time the eigenvectors are used. Asymptotic limits are taken to identify the local expanding and contracting directions, which is a computationally expensive task.

As has already been noted in this introduction, in order to promote feeding currents we can rely on the intrinsic molecular diffusion in the absence of chaotic dynamics. We can directly solve an advection-diffusion equation and monitor the amount of nutrient deposited at some notional mouth. Comparisons are made with the direct solution of the partial differential equation and the inclusion of white noise in the consideration of the map, Oksendal (1985).

The structure of this paper is as follows. In § 2 we derive an area-preserving map which mimics the action of the incompressible Stokes flow due to pulsing point forces (see also the Appendix). Poincaré sections are given and some fixed points of the map (and its repeated composition) are determined. In § 3 we allow the tracer particles to have different properties from the surrounding fluid, and this leads to some inertial effects. Four- and two-dimensional maps are derived and a brief exposition of the resulting structures is given. In § 4 we describe some of the measures used to quantify the level of chaos, and consequently the possible enhancement to mixing. A discussion of the interplay between molecular diffusion and chaotic advection is given in § 5. Finally, in § 6 we present our conclusions.

2. Derivation of a two-dimensional area-preserving map

In this section we propose a two-dimensional area-preserving map which models the motion of a passive tracer in the blinking stokeslet flow field. The flow field is composed of the two vertically aligned stokeslets which are positioned at non-dimensional distances from the plate of $h = 1 + \epsilon$ and $h = 1 - \epsilon$ (in this paper we take $\epsilon = 1/2$). As in the blinking vortex, Aref (1984), and previous work on

the blinking stokeslet, we are required to specify a protocol for switching between the two constituents. Blake & Otto (1996) and Blake *et al.* (1998) exploited a C^1 temporal switching between the configurations, to aid the numerical integration of the system. Here our aim is to reduce the description of the system to a map, and to this end we shall consider each of the stokeslets to pulse with a delta-function form. In a biological context we suggest that this corresponds to assuming that the micro-organism operates over relatively short times; however since we are concerned with a flow which is essentially inertia free the duration of the intervening periods is immaterial. A micro-organism will actually remain in one location for several 'periods' before altering its stalk: this corresponds to an increase in the force (a sequence of pulses actually can be considered to be very similar to a series within this inertia-free context). The temporal variation of the stokeslets is taken to be

$$\Omega_n^{(1\pm\epsilon)}(t;T) = \delta\left(t - T(2n + 1 \mp \tfrac{1}{2})\right),$$

where $n \in \mathbb{Z}$ and $2T$ is the period of the system (the upper stokeslet pulses at $t = T/2$ and the lower one at $t = 3T/2$, and at the corresponding times in the subsequent periods). The stream function for the flow is then

$$\Psi(x,y,t) = \sum_{n=-\infty}^{\infty} \Omega_n^{(1+\epsilon)}(t;T)\psi^{(1+\epsilon)}(x,y) + \Omega_n^{(1-\epsilon)}(t;T)\psi^{(1-\epsilon)}(x,y), \tag{2.1}$$

where

$$\psi^{(1\pm\epsilon)}(x,y) = \alpha^{(1\pm\epsilon)}x\left(\frac{1}{2}\log\left(\frac{x^2 + (y + (1\pm\epsilon))^2}{x^2 + (y - (1\pm\epsilon))^2}\right) - \frac{2(1\pm\epsilon)y}{x^2 + (y + (1\pm\epsilon))^2}\right) \tag{2.2}$$

and we have introduced the following dimensionless parameters:

$$\alpha^{(1\pm\epsilon)} = \frac{F^{(1\pm\epsilon)}T}{4\mu h^2} \quad \text{and} \quad \epsilon = \frac{a}{h},$$

where $\alpha^{(1\pm\epsilon)}$ represents the strength of the respective stokeslets (in this article we shall take $\alpha^{(1+\epsilon)}$ and $\alpha^{(1-\epsilon)}$ to have the same value, in order not to further complicate the problem) and $F^{(1+\epsilon)}$, $F^{(1-\epsilon)}$ are the respective forces of the upper and lower stokeslets. This stream function can be found by using Lorentz's mirror image technique; for details the reader is referred to Blake & Otto (1996), and the references contained therein. As T increases, that is the period of the problem becomes longer, the system is likely to become more chaotic, with the $T \to 0$ limit ($\alpha^{(1\pm\epsilon)} \to 0$) corresponding to the integrable case (it should be recalled that the limit $\epsilon \to 0$ will not necessarily lead to an integrable system). As $T \to 0$ it is as if both features are always turned on and the flow field tends to that corresponding to $\psi^{(1+\epsilon)}(x,y) + \psi^{(1-\epsilon)}(x,y)$. The equations of motion for the tracer are

$$\frac{\mathrm{d}x}{\mathrm{d}t} = \frac{\partial\Psi}{\partial y} \quad \text{and} \quad \frac{\mathrm{d}y}{\mathrm{d}t} = -\frac{\partial\Psi}{\partial x}. \tag{2.3}$$

We now find a discrete map, relating the position of the tracer before the action of the nth pair of pulses with the position after the action of the nth pair of pulses. This will be equivalent to the Poincaré return map obtained by sampling the position of the particle stroboscopically every period, as shown in Blake & Otto (1996) and Blake *et al.* (1998).

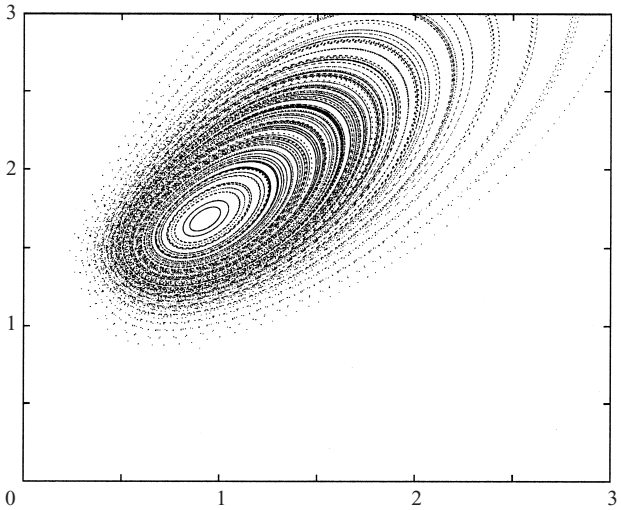

FIGURE 2. Poincaré section for $\alpha^{(1\pm\epsilon)} = 1/5$ (using the midpoint map).

The map associated with the first pulse R_1 is defined as

$$R_1 : \begin{cases} x_{n+1/2} = x_n + \dfrac{\partial \Psi}{\partial y}\left(\dfrac{x_n + x_{n+1/2}}{2}, \dfrac{y_n + y_{n+1/2}}{2}, (2n + \tfrac{1}{2})T\right), \\ y_{n+1/2} = y_n - \dfrac{\partial \Psi}{\partial x}\left(\dfrac{x_n + x_{n+1/2}}{2}, \dfrac{y_n + y_{n+1/2}}{2}, (2n + \tfrac{1}{2})T\right). \end{cases}$$

For the derivation of this map the reader is referred to the Appendix. We also discuss the way in which this map has been made to be area preserving, and the possible ramifications of this choice.

The effect of the other stokeslet is taken into account in the same way and will give rise to a similar map, R_2, incorporating the stream function $\psi^{(1-\epsilon)}$. The full map is then the composition of the two maps $M = R_2 \cdot R_1$. The map $M : (x_n, y_n) \to (x_{n+1}, y_{n+1})$ gives the Poincaré return map for the blinking stokeslet flow, with the stream function defined in (2.2). At this point the technique could be used for any pulsing Stokes flow.

In figures 2, 3, 4 and 5 we show Poincaré sections of the map for $\alpha^{(1\pm\epsilon)} = 1/5$, $3/5$, $4/5$ and 1 respectively. In figures 3, 4 and 5 we also include an enlargement of the area surrounding the fixed point so that some of the resulting structure can be seen. Despite the different protocols similar Poincaré sections were given in Blake & Otto (1996), which were obtained with a C^1 protocol and a symplectic integrator. We see high-order periodic structures and it is possible to determine the corresponding fixed points. The elliptic fixed points are interlaced with hyperbolic points of the same order yielding a heteroclinic structure. The intersection of the unstable and stable manifolds will lead to horseshoe dynamics. For higher values of $\alpha^{(1\pm\epsilon)}$ most of the tori have been destroyed, except for the central one surrounding the fixed point. In figure 6 we show the x and y coordinates of the central fixed point as $\alpha^{(1\pm\epsilon)}$ increases. Also included is information relating to its bifurcation shown by the dotted line, which starts at α_{bif}. This was calculated using the Hénon index (Hénon 1969), which is the condition that the modulus of the trace of the Jacobian matrix becomes greater than 2 or equivalently that the Hessian is negative for the Poincaré map (that is the flow

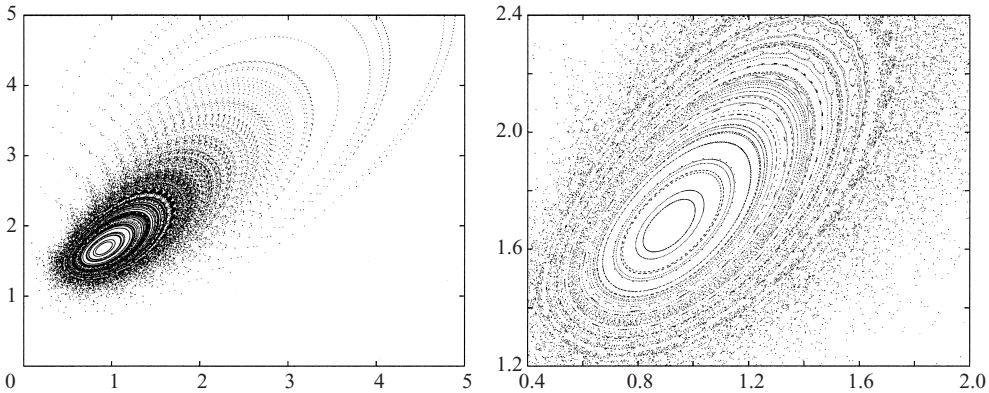

FIGURE 3. Poincaré section for $\alpha^{(1\pm\epsilon)} = 3/5$ with an enlargement of the area surrounding the central fixed point (using the midpoint map).

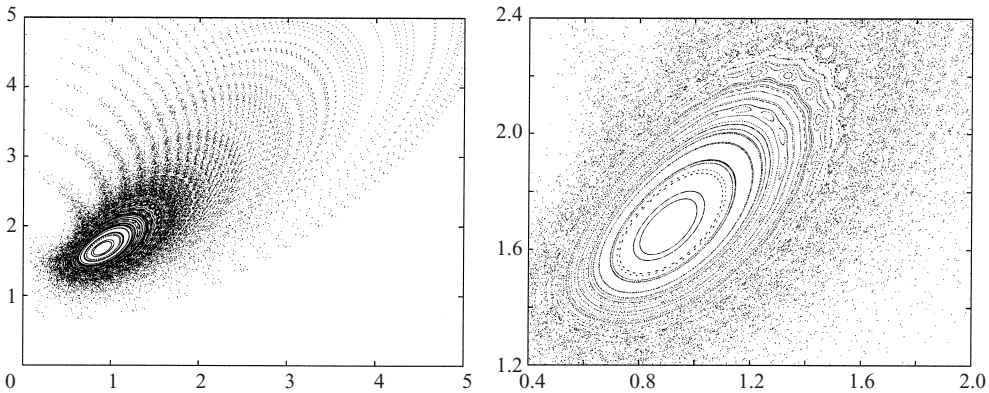

FIGURE 4. Poincaré section for $\alpha^{(1\pm\epsilon)} = 4/5$ with an enlargement of the area surrounding the fixed point (using the midpoint map). Note that the island structures and inherent saddle points which fall between two 'solid' orbits will only lead to a modest degree of mixing, since the particles are still bound by the corresponding tori.

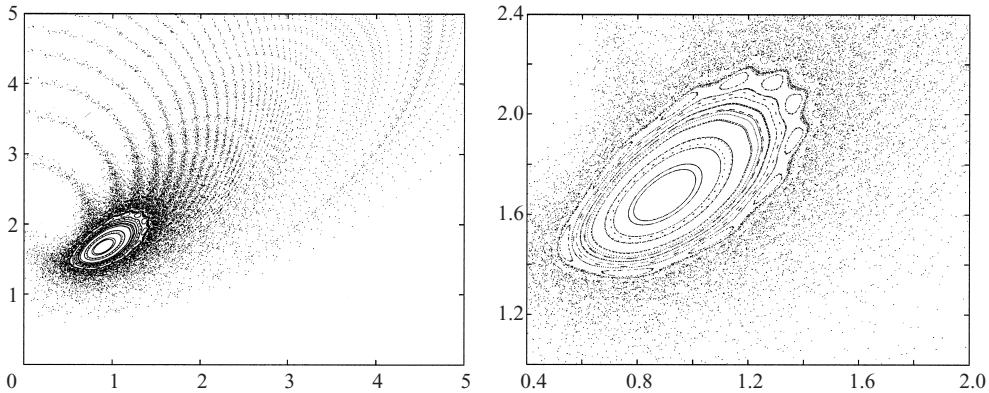

FIGURE 5. Poincaré section for $\alpha^{(1\pm\epsilon)} = 1$ with an enlargement of the area surrounding the fixed point (using the midpoint map).

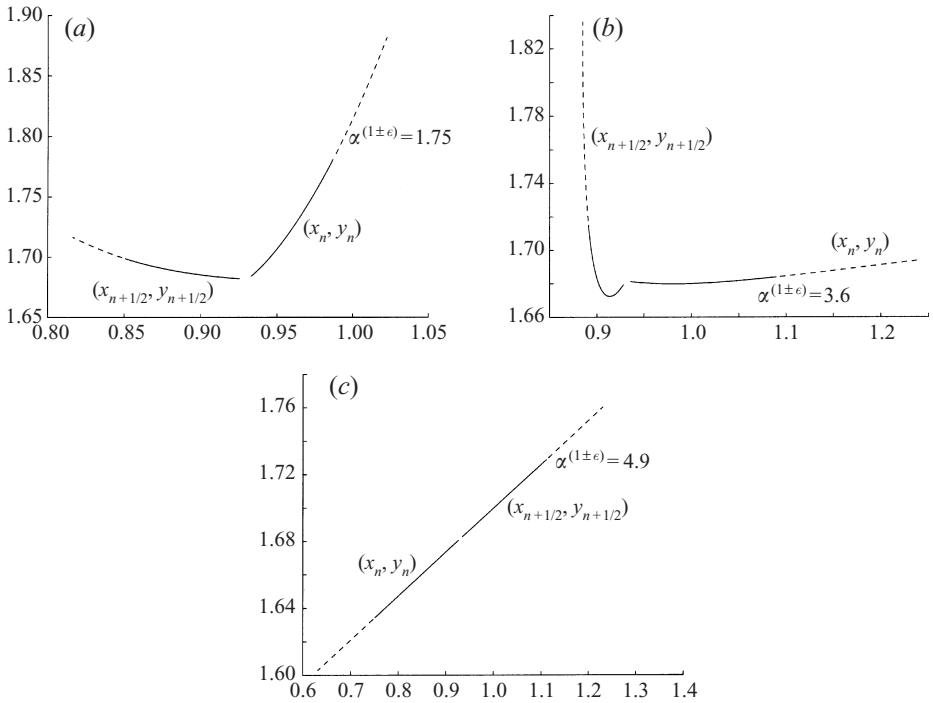

FIGURE 6. Bifurcation diagram for the fixed point of the maps. (*a*) Implicit in x, (*b*) implicit in y, (*c*) midpoint. The dotted line denotes where the modulus of the trace of the Jacobian at the fixed point exceeds 2, that is the Hessian becomes negative. The fixed points are shown for all three variations of the area-preserving map. We recall that these are fixed points of the map M, and not of R_1 and R_2 individually, hence we show (x_n, y_n) and $R_1(x_n, y_n)$. Notice that for small $\alpha^{(1\pm\epsilon)}$ the fixed points are similar, but as this quantity increases they differ, and the central fixed points bifurcate at different values. The fixed points for the midpoint map compare well with Blake & Otto (1996) which exploits a continuous protocol.

in the neighbourhood of the fixed point is one of stretching (hyperbolic) rather than rotation (elliptic)). In Poincaré sections for $\alpha^{(1\pm\epsilon)} > \alpha_{\text{bif}} \approx 7/2$ we find that all the major structure has been destroyed (such a Poincaré section is shown later in figure 13). It should be noted that there will always be elliptic points surrounded by regions of integrability; however the area of these regions may contract to be extremely small. This can be observed when considering small areas of apparently chaotic parts of the phase space. We now consider the influence of inertial effects on the particle motion.

3. A map for finite-size particles in the blinking stokeslet flow

In this section we will consider inertial effects due to the finite size of the particles and the fact that they may have a different density than that of the surrounding fluid. For example such objects could be heavy particles or spherical bubbles.

The velocity $\boldsymbol{v}$ of such particles will be given by the (approximate) differential equation

$$\frac{\mathrm{d}\boldsymbol{v}}{\mathrm{d}t} = \lambda(\boldsymbol{u} - \boldsymbol{v}) + \frac{3R}{2}\frac{\partial \boldsymbol{u}}{\partial t} + R(\boldsymbol{u} + \tfrac{1}{2}\boldsymbol{v}) \cdot \nabla \boldsymbol{u} \tag{3.1}$$

where

$$\lambda = \frac{6\pi a\mu}{m_p + \frac{1}{2}m_f} \quad \text{and} \quad R = \frac{m_f}{m_p + \frac{1}{2}m_f}$$

and a is the radius of the particle, μ is the dynamic viscosity of the fluid, m_f is the mass of the displaced fluid and m_p is the mass of the spherical particle. The parameters in (3.1) are the timescale for inertial effects λ and the mass ratio R. Notice that for $R > 2/3$ the particles are lighter than the fluid and vice versa for $R < 2/3$. The position of the particle is given by

$$\frac{\mathrm{d}\boldsymbol{r}}{\mathrm{d}t} = \boldsymbol{v}. \tag{3.2}$$

This model was proposed by Maxey & Riley (1983), is extended in Maxey (1990) and has been used recently in Maxey *et al.* (1997). We should note two interesting limits:

(*a*) the limit of aerosol particles where m_f and R are both taken to be zero, and

(*b*) the limit of spherical gas bubbles where $m_p = 0$ and $R = 2$.

Examples of both of these limits will be given in due course. Also of interest is the quantity λ^{-1} which is the inertial response time. If we take $\lambda \to \infty$ then we obtain $\boldsymbol{v} = \boldsymbol{u}$ so that the particles follow the streamlines. This will be the appropriate limit for many filter feeding processes.

Our objective in this section is to obtain a map for the motion of particles with inertia in the blinking stokeslet flow field. We define the new variable $\boldsymbol{v} = \exp(-\lambda t)\boldsymbol{v}_c$. For this new function, equation (3.1) becomes

$$\frac{\mathrm{d}\boldsymbol{v}_c}{\mathrm{d}t} = \lambda \exp(\lambda t)\boldsymbol{u} + \frac{3R}{2}\exp(\lambda t)\frac{\partial \boldsymbol{u}}{\partial t} + R\exp(\lambda t)(\boldsymbol{u} + \tfrac{1}{2}\boldsymbol{v})\cdot\nabla\boldsymbol{u}. \tag{3.3}$$

We notice that for the flow field defined by the stream function (2.1), $\boldsymbol{v}_c$ will be a constant for $t < \frac{1}{2}T + 2nT$ and also a (different) constant for $\frac{1}{2}T + 2nT < t < \frac{3}{2}T + 2nT$. To find the change in this constant we will have to integrate through the delta functions which leads to Heaviside functions. Defining $\boldsymbol{v}_{c_n} = \boldsymbol{v}_c(\frac{1}{2}T + 2nT_-)$ and $\boldsymbol{v}_{c_{n+1/2}} = \boldsymbol{v}_c(\frac{3}{2}T + 2nT_-) = \boldsymbol{v}_c(\frac{1}{2}T + 2nT_+)$ we find that

$$\boldsymbol{v}_{c_{n+1/2}} - \boldsymbol{v}_{c_n} = \exp(\lambda(2nT + \tfrac{1}{2}T))\{\lambda\boldsymbol{u} - \tfrac{3}{2}R\lambda\boldsymbol{u} + R(\boldsymbol{u} + \tfrac{1}{2}\boldsymbol{v})\cdot\nabla\boldsymbol{u}\}(t = 2nT + \tfrac{1}{2}T)$$

where all these terms are evaluated at $t = 2nT + \frac{1}{2}T$ and the second term on the right-hand side arises from integrating the term $\frac{3}{2}R\exp(\lambda t)\partial\boldsymbol{u}/\partial t$ by parts with respect to time. Another term arises from this integration but instead of leading to a Heaviside function yields another delta function. In the velocity map this plays no rôle; however, when we obtain the spatial component of the map this leads to an extra term, which corresponds to the term found in the standard two-dimensional map. The term $\boldsymbol{u}|_{(t=2nT+T/2)}$ will be taken as $\boldsymbol{u}(x_m, y_m)$ as before (where (x_m, y_m) is defined below as the arithmetic mean of the two endpoints), and similarly for the other functions. The reason for this choice is so that the map reverts to being area preserving in the limit $\lambda \to \infty$.

We return to the original coordinates and obtain

$$\boldsymbol{v}_{n+1/2}e^{\lambda T} - \boldsymbol{v}_n = \lambda(1 - \tfrac{3}{2}R)\boldsymbol{u}(x_m, y_m) + R(\boldsymbol{u}(x_m, y_m) + \tfrac{1}{2}\boldsymbol{v}_n)\cdot\nabla\boldsymbol{u}(x_m, y_m), \tag{3.4}$$

where $\boldsymbol{v}_{n+1/2} = \boldsymbol{v}(\frac{3}{2}T + 2nT_-) \neq \boldsymbol{v}(\frac{1}{2}T + 2nT_+)$ and $(x_m, y_m) = ((x_n + x_{n+1/2})/2, (y_n + y_{n+1/2})/2)$. On integrating the equation for $\boldsymbol{r}$, which we may rewrite as

$$\frac{\mathrm{d}\boldsymbol{r}}{\mathrm{d}t} = e^{-\lambda t}\boldsymbol{v}_c + \tfrac{3}{2}R\delta(t - (2nT + \tfrac{1}{2}T/2))\boldsymbol{u},$$

where we have integrated from $2nT + \frac{1}{2}T - \epsilon_1$ to $2nT + \frac{3}{2}T - \epsilon_1$, and taking into account that $\boldsymbol{v}_c$ is a constant for $t < 2nT + \frac{1}{2}T$ and a (different) constant for $2nT + \frac{1}{2}T < t < 2nT + \frac{3}{2}T$ we obtain

$$\begin{aligned}\boldsymbol{r}(2nT + \tfrac{3}{2}T - \epsilon_1) - \boldsymbol{r}(2nT + \tfrac{1}{2}T - \epsilon_1)\\ = \boldsymbol{v}_{c_n} \int_{2nT+T/2-\epsilon_1}^{2nT+T/2} \mathrm{e}^{-\lambda t}\,\mathrm{d}t + \boldsymbol{v}_{c_{n+1/2}} \int_{2nT+T/2}^{2nT+3T/2-\epsilon_1} \mathrm{e}^{-\lambda t}\,\mathrm{d}t\\ + \frac{3R}{2} \int_{2nT+T/2-\epsilon_1}^{2nT+3T/2-\epsilon_1} \delta(t - (2nT + T/2))\boldsymbol{u}\,\mathrm{d}t.\end{aligned}$$

Taking the limit $\epsilon_1 \to 0$ we obtain

$$\boldsymbol{r}_{n+1/2} - \boldsymbol{r}_n = \frac{\mathrm{e}^{\lambda T} - 1}{\lambda}\boldsymbol{v}_{n+1/2} + \frac{3R}{2}\boldsymbol{u}(x_m, y_m). \tag{3.5}$$

We can now look at the behaviour of the system as $\lambda \to \infty$. In this case from (3.4) we find that

$$\boldsymbol{v}_{n+1/2} \simeq \lambda \mathrm{e}^{-\lambda T}\boldsymbol{u}(x_m, y_m)(1 - \tfrac{3}{2}R)$$

and from (3.5) we obtain that

$$\boldsymbol{r}_{n+1/2} - \boldsymbol{r}_n \simeq (1 - \mathrm{e}^{-\lambda T})\boldsymbol{u}(x_m, y_m)(1 - \tfrac{3}{2}R) + \tfrac{3}{2}R\,\boldsymbol{u}(x_m, y_m),$$

so that in the limit as $\lambda T \to \infty$,

$$\boldsymbol{r}_{n+1/2} - \boldsymbol{r}_n \simeq \boldsymbol{u}(x_m, y_m),$$

which is the area-preserving map we obtained for the passive tracer. All the dissipative effects in the motion of the tracer are then introduced by the difference of density of the particles and the fluid, and by their finite size.

Similar results hold for the other stokeslet. In coordinate form we propose the following maps S_i, $i = 1, 2$ (from (3.4) and (3.5)), where

$$\left.\begin{aligned} v'_{1,i}\,\mathrm{e}^{\lambda T} - v_{1,i} &= \lambda(1 - \tfrac{3}{2}R)\frac{\partial \psi_i}{\partial y} + R\left(\frac{\partial \psi_i}{\partial y} + \tfrac{1}{2}v_{1,i}\right)\frac{\partial^2 \psi_i}{\partial x \partial y} + R\left(-\frac{\partial \psi_i}{\partial x} + \tfrac{1}{2}v_{2,i}\right)\frac{\partial^2 \psi_i}{\partial y^2},\\ v'_{2,i}\,\mathrm{e}^{\lambda T} - v_{2,i} &= -\lambda(1 - \tfrac{3}{2}R)\frac{\partial \psi_i}{\partial x} - R\left(\frac{\partial \psi_i}{\partial y} + \tfrac{1}{2}v_{1,i}\right)\frac{\partial^2 \psi_i}{\partial x^2} - R\left(-\frac{\partial \psi_i}{\partial x} + \tfrac{1}{2}v_{2,i}\right)\frac{\partial^2 \psi_i}{\partial x \partial y},\\ x'_i - x_i &= \frac{\mathrm{e}^{\lambda T} - 1}{\lambda}v'_{1,i} + \tfrac{3}{2}R\frac{\partial \psi_i}{\partial y},\\ y'_i - y_i &= \frac{\mathrm{e}^{\lambda T} - 1}{\lambda}v'_{2,i} - \tfrac{3}{2}R\frac{\partial \psi_i}{\partial x}, \end{aligned}\right\}$$

where $x'_1 = x_{n+1/2} = x_2$, $x'_2 = x_{n+1}$, $x_1 = x_n$ (and similarly for y), $\psi_1 = \psi^{(1+\epsilon)}$ and $\psi_2 = \psi^{(1-\epsilon)}$ (all functions are evaluated at the midpoint of the corresponding interval). The Poincaré map in this case is the composition of S_1 and S_2 so that $\tilde{M} = S_2 \cdot S_1$. This is a four-dimensional dissipative map.

We have shown that as $\lambda \to \infty$ this four-dimensional map reverts to the inertia-free map. Here we shall determine the leading-order correction to the inertia map, which

occurs at $O(\lambda^{-1})$. We can see that the local particle velocity will be given by

$$\boldsymbol{v} = \boldsymbol{u} + \gamma \left(\frac{\partial \boldsymbol{u}}{\partial t} + \boldsymbol{u} \cdot \nabla \boldsymbol{u} \right)$$

where γ is of order λ^{-1} and is given by

$$\gamma = \frac{2a^2}{9\nu} \frac{\rho_f - \rho_p}{\rho_f}$$

where we use the density of the fluid and the tracer, instead of their masses. This reduction is given in detail in Druzhinin & Ostrovsky (1994).

A particle moving in a fluid with density different from the particle density will experience forces due to inertia. The theory of Druzhinin & Ostrovsky (1994) shows that a characteristic time scale for transport effects due to inertia is $\tau_i = 1/\epsilon^2$ where $\epsilon = a^2 U_0 / L\nu$ and a is the radius of the particle, U_0 a characteristic velocity magnitude in the external flow, L a characteristic length scale and ν the kinematic viscosity of the fluid. On the other hand if molecular diffusion is present we have a diffusive time scale of the form $\tau_D = L^2/D_0$. If $\tau_D \approx \tau_i$ then both inertial effects and diffusive effects must be taken into account, Yannacopoulos, Rowlands & King (1999).

We can now use this approximation for the pulsed flow and obtain a two-dimensional dissipative map $\hat{S}_i$, $i = 1, 2$, of the form

$$x_i' - x_i = \frac{\partial \psi_i}{\partial y} + \gamma \left\{ \frac{\partial \psi_i}{\partial y} \frac{\partial^2 \psi_i}{\partial x \partial y} - \frac{\partial \psi_i}{\partial x} \frac{\partial^2 \psi_i}{\partial y^2} \right\},$$

$$y_i' - y_i = -\frac{\partial \psi_i}{\partial x} + \gamma \left\{ -\frac{\partial \psi_i}{\partial y} \frac{\partial^2 \psi_i}{\partial x^2} + \frac{\partial \psi_i}{\partial x} \frac{\partial^2 \psi_i}{\partial x \partial y} \right\},$$

where the same conventions as for the four-dimensional map are taken and the Poincaré map is the composition $\hat{M} = \hat{S}_2 \cdot \hat{S}_1$. This map is area-preserving when $\gamma = 0$ and all dissipative effects are introduced by particle inertia. In fact most of the dynamics of the system can be realized using the two-dimensional map. These effects are summarized as when the particle is lighter ($R > 2/3$) than the fluid its path will tend towards the fixed point and when it is heavier ($R < 2/3$) it will spiral out. In both cases there are no longer closed tori. The additional dynamics included in the four-dimensional map is the delay of the system in reacting to changes. For instance if the particle is given an initial velocity different from the local average velocity the amount of time for it to tend to the orbits with $\lambda \to \infty$ is dependent on $1/(\lambda T)$. This is demonstrated by three particles all starting from the point $(x_0, y_0) = (3, 3)$ shown in figure 7 with velocities given by $((\psi_1 + \psi_2)_y, -(\psi_1 + \psi_2)_x)$ and $(-3, 2)$. All trajectories are shown for $T = 0.1$ and with $R = 2/3$, which corresponds to the particle having the same mass as the displaced fluid. The solid line corresponds to a particle in a flow with $\lambda = 100$, and the plus signs and circles to particles in a flow with $\lambda = 10$. As well as the fact that the line tends to the inertia free streamlines faster, we also observe that for moderate λ the particles in fact spiral inward despite their mass, which is very significant in the context of filter feeding. In figure 8 we show Poincaré sections for $R = 0$ and $R = 2$ (both calculations use a value of $\lambda = 10$). We observe the trends that the aerosol particles spiral outwards, whereas the spherical gas bubbles become trapped within the central eddy. It is only the influence of non-infinite inertial response time which goes against this trend. We now include a discussion of the measures which allow us to quantify the level of mixing present, caused by the chaotic structures.

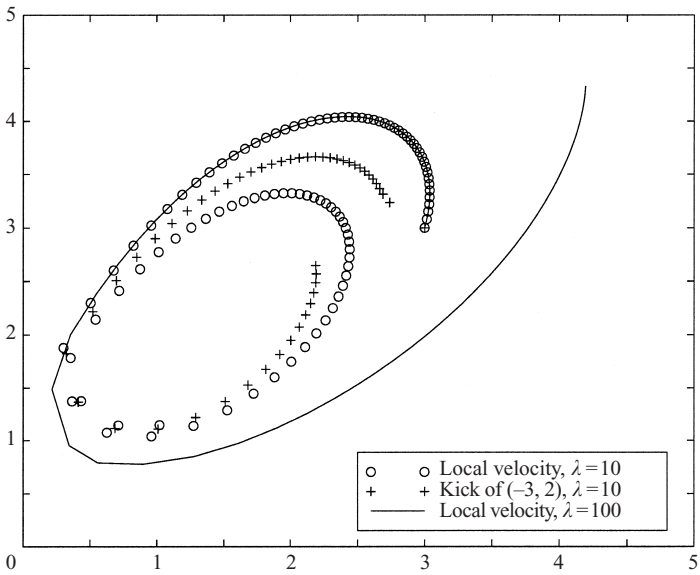

FIGURE 7. The paths of three particles all starting at (3, 3) with $R = 2/3$, $\alpha^{(1\pm\epsilon)} = 3/4$ and $T = 1/10$. The first particle (circles) starts with an average local velocity ($\lambda = 10$) and the second (plus signs) starts with a kick of $(-3, 2)$ ($\lambda = 10$). The third has an average local velocity with $\lambda = 100$.

4. Measures used to study the dynamics of the system

In order to determine the structure of the phase space we will exploit the following techniques. One of the classical measures of chaos is the Lyapunov exponent (LE), which is a measure of exponential local instability in the phase space, which is a sign of chaos. This instability means that nearby orbits in phase space diverge exponentially and this implies 'randomization' or memory loss in the system. The LE is defined as

$$\lambda_{LE} = \lim_{t\to\infty} \frac{1}{t} \ln\left(\frac{\|\delta \boldsymbol{x}(t)\|}{\|\delta \boldsymbol{x}(0)\|}\right),$$

where $\delta \boldsymbol{x}$ is the deviation from an orbit of the system. For a vector field $\boldsymbol{v}$ the deviation is governed by the linearized system

$$\dot{\delta \boldsymbol{x}} = \nabla \boldsymbol{v} \delta \boldsymbol{x} = \boldsymbol{J} \delta \boldsymbol{x},$$

where $\boldsymbol{J}$ is the Jacobian for the dynamical system. The definition of the LE is similar for a mapping. The condition that $\lambda_{LE} > 0$ is one of the usual definitions of chaos.

However, the limit $t \to \infty$ is often not very useful or practical to achieve. Another interesting quantity is the local Lyapunov exponent (LLE) or finite-time Lyapunov exponent, Eckhardt & Yao (1993). The LLE is defined as

$$\lambda_{LLE}(\boldsymbol{x}_0, t) = \frac{1}{t} \ln\left(\frac{\|\delta \boldsymbol{x}(t)\|}{\|\delta \boldsymbol{x}(0)\|}\right),$$

where $\boldsymbol{x}_0$ is the initial point of a trajectory and $\delta \boldsymbol{x}$ is the divergence of a nearby orbit from this trajectory. This is essentially the average rate of exponential stretching experienced by a fluid element after time t. This definition is useful as it allows us to consider stretching in a flow as a local (space-dependent) quantity. In principle, stretching in realistic fluid flows is a very non-uniform process and one encounters regions of very high or very low stretching, which are related to the mixed properties

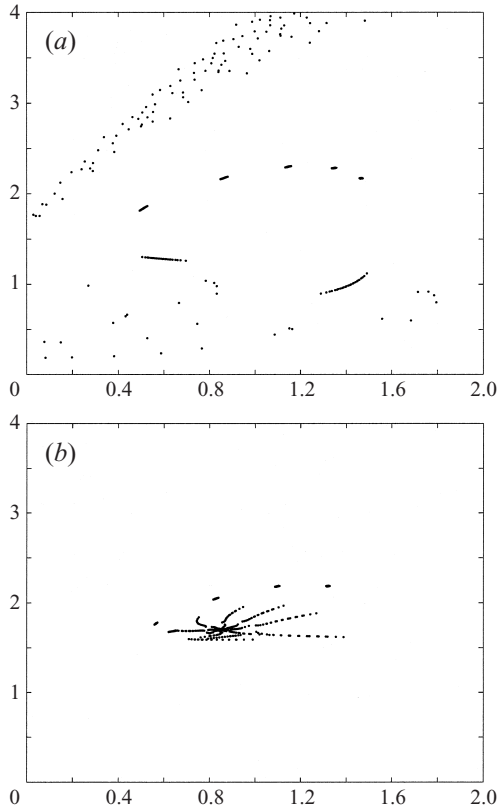

FIGURE 8. Poincaré section for $\lambda = 10$ with an initial point $(1.5, 2)$ and $\alpha^{(1\pm\epsilon)} = 1.4$. (*a*) $R = 0$, aerosol (massive), (*b*) $R = 2$, gas bubbles (massless). Notice that all the points are drawn into the centre of the eddy for $R = 2$ and expelled for $R = 0$ (all particles are all given zero initial velocity).

of phase space or the pathlines of the flow (regions of chaos intermingled with regions of regular orbits). The LLE will converge to LE as $t \to \infty$. In principle the LE will also depend on space but in ergodic regions (as the connected chaotic regions are usually considered to be) the LE will be independent of initial condition almost everywhere (in a measure theoretic sense). Under the assumptions of ergodicity a point will eventually visit every point of the region, which implies that the average over time is equivalent to the spatial average: the Lyapunov exponent will be independent of the initial point, provided the system has been considered for long enough times. This represents one of the limitations of the consideration of LE. As noted earlier there will always be islands of integrability and any region incorporating one of these cannot be considered to be ergodic.

The LLE is related to the eigenvalues of the Jacobian matrix for a flow (or their logarithms for a map). Furthermore, even though it is evident, we note here that a ball of tracer in the flow will be deformed after time T into an ellipsoid with major axis $\exp(\lambda_{LLE} T)$ where λ_{LLE} is the LLE. The basic algorithm to compute the LE and LLE involves tracking a point and calculating the Jacobian $\boldsymbol{J}_{R_2}\boldsymbol{J}_{R_1}$. The eigenvalues are then calculated; notice that since the map is area preserving the product of the eigenvalues is unity which implies that the local action of the map is either purely a rotation, or a stretching and contraction. We look for the logarithm of the maximum magnitude of the eigenvalues. The total exponent is given by the time-average of these quantities.

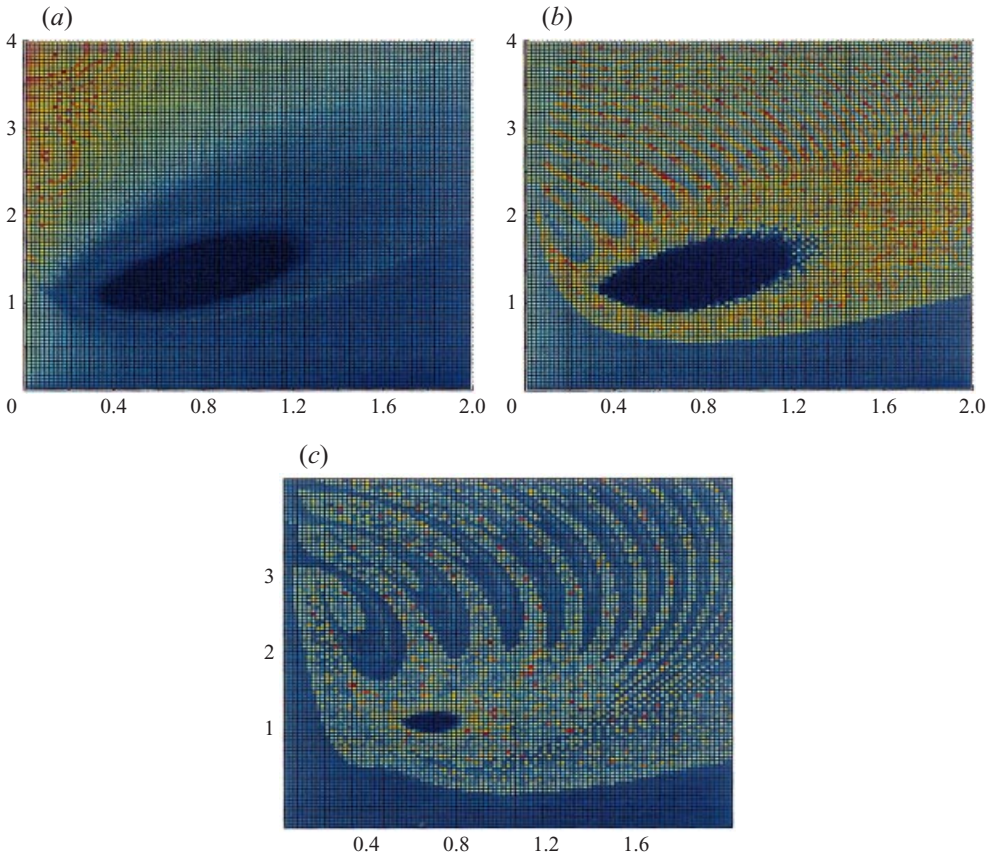

FIGURE 9. Local Lyapunov exponents for (*a*) $\alpha^{(1\pm\epsilon)} = 1/10$, $\max(\lambda_{LLE}) = 0.1183$, (*b*) $\alpha^{(1\pm\epsilon)} = 3/4$, $\max(\lambda_{LLE}) = 0.2268$, (*c*) $\alpha^{(1\pm\epsilon)} = 3/2$, $\max(\lambda_{LLE}) = 0.3827$. The values have been averaged over 100 periods of the map. The colour maps are relative, and the maximum values of the LLEs are given in the individual captions.

In figure 9 we show the LLE for one hundred periods. The grid contains 100 by 100 points and demonstrates the dominant structures. For instance around the central fixed point there is very little stretching, as the flow here is main rotational. Similarly in the neighbourhood of $y = 0$ there is very little stretching. Notice also the 'stripes' above the vortex core, in which there is relatively low stretching. We include the LLEs for three different values of $\alpha^{(1\pm\epsilon)}$. We note that for low values the particles, which are well mixed, originate above the stokeslets' locations. For intermediate values we see that the mixing has been extended, although a central core exists around the fixed point in which the action of the map is largely rotational. In the final figure we show a case where most of the region will be mixed. In these figures we also give the values of $\max(\lambda_{LLE})$ over the region (since the colour scaling is relative). We now clearly see that an increase in $\alpha^{(1\pm\epsilon)}$ corresponds to additional mixing.

The chaotic nature of the dynamics can lead to enhanced transport in the flow. In a flow with regular streamlines, the tracer is restricted onto tori (defined by the streamlines) and so a great part of phase space (which coincides with physical space in problems of this kind) is inaccessible to it. In this case the tracer can visit certain parts of phase space only under the effect of molecular diffusion. However, in the

case where the motion of the tracer is chaotic, the tori onto which the streamlines are confined are broken, and this leads to a connection of certain parts of phase space otherwise inaccessible in the absence of molecular diffusion.

These ideas can be formalized by saying that chaos can lead to enhanced transport, which in certain cases can be modelled by the use of diffusion processes. One important question is the connection of these diffusion coefficients with the characteristics of the flow or its dynamical characteristics, for instance the LE, or the LLE. This problem is a very interesting and technically difficult one that has attracted the interest of both the dynamical systems and the fluid mechanics communities, Wiggins (1992) and Yannacopolous & Rowlands (1997). Rigorous results have only been obtained for very idealized cases, but here without trying to be rigorous we will attempt to present some arguments on how we can derive enhanced transport coefficients from dynamical characteristics of the system. First let us summarize a very transparent argument of Ott and coworkers, see for instance Antonsen & Ott (1991) and Varosi, Antonsen & Ott (1991). In the absence of molecular diffusion the gradient of a scalar field Φ (i.e. concentration) will satisfy the conservation law

$$\frac{\mathrm{d}}{\mathrm{d}t}(\delta \boldsymbol{x} \cdot \nabla \Phi) = 0,$$

where $\delta \boldsymbol{x}$ is the deviation from an orbit. Since $\delta \boldsymbol{x}$ decreases exponentially in some directions of the flow, for conservation we require that $\nabla \Phi$ should increase exponentially along these directions. Thus we expect

$$| \nabla \Phi | \sim \exp(t\lambda(\boldsymbol{x}_0, t)),$$

which implies large variations of the gradient from point to point in the flow. Regions with high LLE will then be regions with high concentration gradients. Now consider also the effect of molecular diffusion on the tracer. Since the diffusive current is proportional to the concentration gradient, regions of high LLE will correspond to high diffusive current and this will lead to a large effective diffusivity. This essentially 'hand-waving' argument will lead us to a basic understanding of why chaos can lead to enhanced diffusion in a real situation (i.e. in the presence of molecular diffusion). As proved by Ott and coworkers, in the absence of molecular diffusion $\nabla \Phi$ will tend to concentrate on a fractal set and the fractal exponents of this set will be related to the distribution of the LLE. Naturally, molecular diffusion will tend to smooth this structure.

One can offer a number of alternative approaches to understand this result. We switch to the study of discrete maps rather than continuous flows. Consider a map which has an expanding and a contracting direction and includes some extrinsic stochasticity (e.g molecular diffusion) acting on the system. Consider the map

$$x_{n+1} = \Lambda x_n + \xi_n, \qquad y_{n+1} = \Lambda^{-1} y_n + \xi_n,$$

where ξ_n are identically distributed Gaussian variables with zero mean and standard deviation D, and $\Lambda > 1$. By iterating the map we can obtain in the expanding direction

$$x_n = \Lambda^n x_0 + \sum_{m=0}^{n-1} \Lambda^{n-1-m} \xi_m.$$

Averaging over the white noise terms we can get the mean position

$$\langle x_n \rangle = \Lambda^n x_0$$

and by squaring and averaging we get

$$\langle x_n^2 \rangle = \Lambda^{2n} x_0^2 + D \sum_{m=0}^{n-1} \Lambda^{2(n-1-m)} = \Lambda^{2n} x_0^2 + D \frac{\Lambda^{2n} - 1}{\Lambda^2 - 1}.$$

The dispersion from the mean trajectory is then given by

$$\langle x_n^2 \rangle - \langle x_n \rangle^2 = D \frac{\Lambda^{2n} - 1}{\Lambda^2 - 1},$$

which is exponentially growing in time but for small n it can be approximated as

$$\langle x_n^2 \rangle - \langle x_n \rangle^2 \sim \frac{2D}{\Lambda^2 - 1} n \ln \Lambda.$$

We can define a diffusion coefficient in an alternative way as the pre-factor for the linear growth of the dispersion. Such a definition makes sense for small n and will lead to

$$D_e = \frac{2D}{\Lambda^2 - 1} \ln \Lambda$$

which is proportional to the LE. More detailed and rigorous discussion of this result can be found in Bohr & Rand (1987) and Gaspard & Nicolis (1990).

The above rather informal argument seems to be supported by the results of Tang & Boozer (1996) who solve the advection–diffusion equation in Lagrangian coordinates for the Arnol'd cat map which is a purely hyperbolic dynamical system. According to their results an initial probability distribution keeps its initial spatial dependence for up to time $t_a = \ln(2\Omega)/2\lambda$ (in the expanding direction) and then the spatial dependence is damped during a short interval $1/\lambda$, where λ is the LE and $\Omega = \lambda L^2/D$ (L is a characteristic spatial scale for the initial probability distribution). The time scale $1/\lambda$ is a characteristic one which can be compared to the diffusive time scale $t_d = L^2/D$. By this argument we can assume that we will have an effective diffusivity which will be proportional to the LE λ.

Having introduced the connection between chaos and transport we wish to quote here some further results by Tang & Boozer (1996) connecting the geometry of stretching and contraction of the phase space to transport under the combined effects of advection and molecular diffusion. Tang & Boozer (1996) define the metric tensor in Lagrangian coordinates as

$$\boldsymbol{g} = \boldsymbol{J}\boldsymbol{J}^T$$

where $\boldsymbol{J}$ is the Jacobian of the map (the quantity $\boldsymbol{g}$ is known as the left Cauchy–Green strain tensor). The metric tensor is a symmetric matrix which has two distinct eigenvalues corresponding to an expanding and a contracting direction and hence can be diagonalised as

$$\boldsymbol{g} = \Sigma \boldsymbol{e}\boldsymbol{e} + \Sigma^{-1} \boldsymbol{s}\boldsymbol{s}$$

where $\Sigma > 1$ and dyadic notation has been used. The LLE is given in terms of Σ as

$$\lambda(\boldsymbol{x}, t) = \frac{\ln(\Sigma(\boldsymbol{x}, t))}{t}$$

and the limit as $t \to \infty$ tends to LE. As $t \to \infty$ the vectors $\mathbf{e}$ and $\mathbf{s}$ tend to their asymptotic values $\boldsymbol{e}_\infty$ and $\boldsymbol{s}_\infty$. According to Tang & Boozer transport as a result of advection and diffusion is related to the field lines of the vector field $\boldsymbol{s}_\infty$. The major barriers to transport are related to the sharp bends of these field lines and the

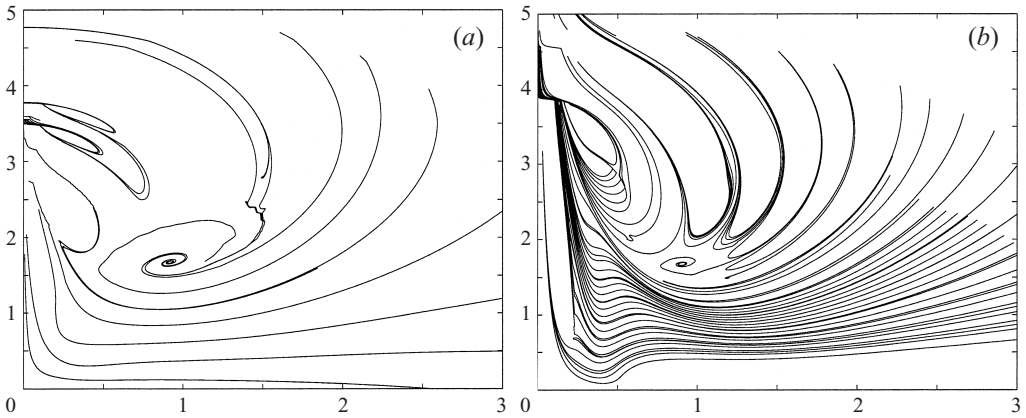

FIGURE 10. Stable foliation lines shown for (*a*) $\alpha^{(1\pm\epsilon)} = 1/2$ and (*b*) 3/2.

curvature of the vector field defined by $\boldsymbol{k}_s = \boldsymbol{s}_\infty \cdot \nabla s_\infty$ (a similar definition can give the curvature $\boldsymbol{k}_e$ of the vector field $\boldsymbol{e}_\infty$). The transport barriers are centred in the regions where

$$\boldsymbol{k}_e = \boldsymbol{0} \quad \text{and} \quad \nabla \cdot \boldsymbol{k}_e > 0.$$

The transport barriers are approximately bounded by the curve satisfying

$$\nabla \cdot \boldsymbol{k}_e + k_e^2 = 0, \quad k_e \geqslant \bar{k},$$

where $\bar{k}$ is the average curvature of the *s*-line. In figures 10(*a*) and 10(*b*) we display the *s* lines computed for the blinking stokeslet system for $\alpha^{(1\pm\epsilon)} = 1/2$ and 3/2 respectively. In order to find the *s*-line starting at the point (x_0, y_0), we calculate the point (x_1, y_1) and the Jacobian defined in (A 1) which allows us to construct $\boldsymbol{g}$. If the action of the map is one of rotation the eigenvalues are both unity (and $\boldsymbol{g}$ is the identity); if not we can determine the expanding and contracting directions, $\boldsymbol{e}$ and $\boldsymbol{s}$ respectively. We require that the direction does not change more than $\pi/2$ so that we always integrate in the same sense. We proceed to determine (x_2, y_2), and subsequently the metric tensor associated with this iteration of the map. The composite metric tensor is formed and we again determine $\boldsymbol{e}$ and $\boldsymbol{s}$. If the direction does not change by more than some pre-defined tolerance we claim to have attained the limits $\boldsymbol{e}_\infty$ and $\boldsymbol{s}_\infty$. This process is very expensive, especially close to the central elliptic fixed point, since the action of the map is mainly one of rotation. Once we have determined the asymptotic directions we integrate using a simple Euler step in the $\boldsymbol{s}_\infty$-direction. Notice the agreement between this and the local Lyapunov exponents shown in figure 9: note that the regions of high curvature correspond to local minima of LLE, Tang & Boozer (1996). This measure is linked to the stretching efficiency defined in Ottino (1989).

Finally, to close this section we wish to bring to attention the possibility of anomalous transport as an effect of the dynamics. In such cases the transport in phase space is no longer diffusive and this is best shown in the dispersion of tracer as a function of time in space. The dispersion in general behaves as

$$\langle x_n^2 \rangle - \langle x_n \rangle^2 \sim n^{\beta_{xx}}, \quad \langle y_n^2 \rangle - \langle y_n \rangle^2 \sim n^{\beta_{yy}} \quad \text{and} \quad \langle x_n y_n \rangle - \langle x_n \rangle \langle y_n \rangle \sim n^{\beta_{xy}},$$

where the β will be called the transport exponents. It is frequent for transport to be non-diffusive, i.e $\beta \neq 1$. If $\beta > 1$ the transport is called superdiffusive whereas if $\beta < 1$

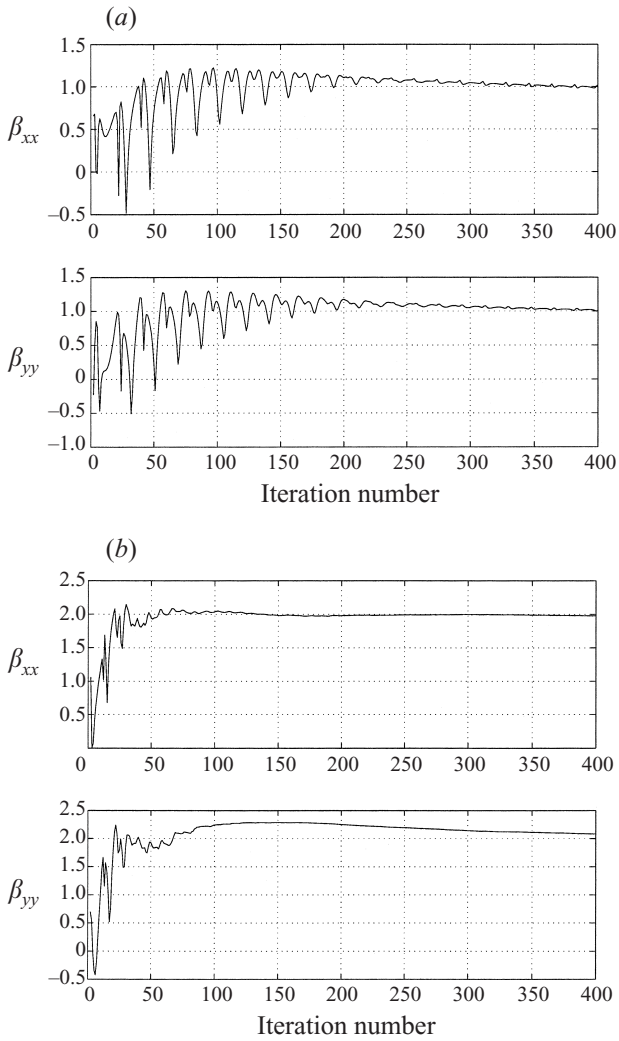

FIGURE 11. Horizontal and vertical dispersion for a blob above the core of the eddy for (*a*) $\alpha^{(1\pm\epsilon)} = 3/5$ and (*b*) $\alpha^{(1\pm\epsilon)} = 6/5$ (shown for 400 iterations). Both cases use the same initial distribution of particles. The values of β are calculated by simply normalizing the initial particle distribution and using logarithms.

it is called subdiffusive. In this paper we examine the possibility of such anomalous transport for the blinking stokeslet flow. We show the variation of dispersion in figure 11. An initial blob of 121 particles is placed above the core of the eddy. The runs were repeated with white noise and the consequent diffusion was further enhanced by the chaotic advection, as might be expected from the calculations in the absence of the noise, as shown in figure 12.

The particles are placed quite close to the fixed point, and although the Poincaré section in the former case shows evidence of chaos the particles remain within a relatively narrow band. In figure 13 we show a Poincaré section for $\alpha^{(1\pm\epsilon)} = 5/2$, this clearly shows the dispersion of particles away from the central fixed point. The values of β vary spatially and thus the numbers given above are purely representative.

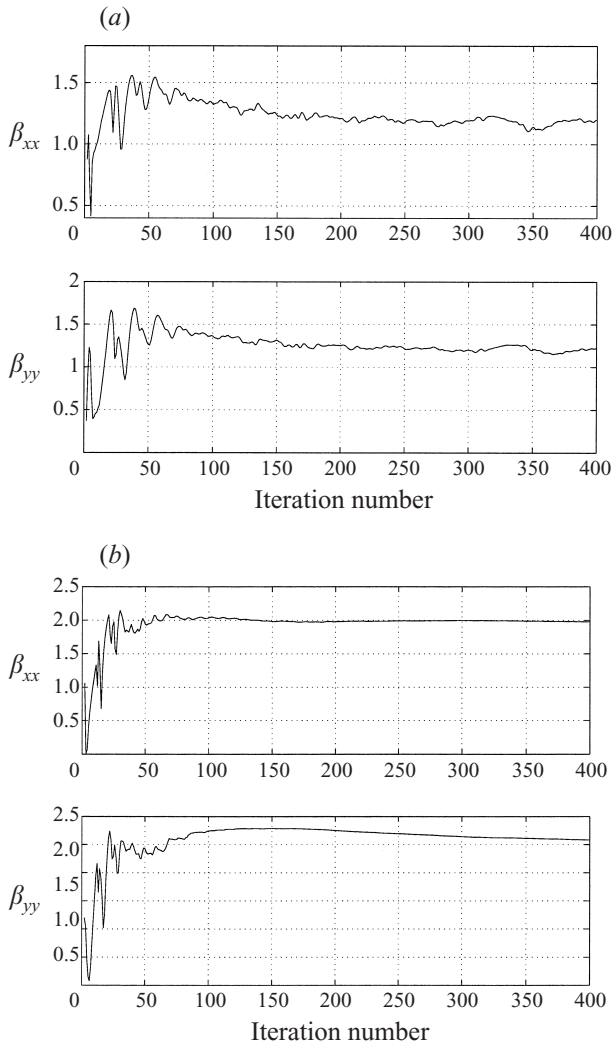

FIGURE 12. Horizontal and vertical dispersion for a blob above the core of the eddy for (*a*) $\alpha^{(1\pm\epsilon)} = 3/5$ and (*b*) $\alpha^{(1\pm\epsilon)} = 6/5$ (shown for 400 iterations). These are the same runs as shown in figure 11 but with additional white noise terms, corresponding to molecular diffusion. Note in comparison with the corresponding sub figures of figure 11 we unsurprisingly observe a slight increase in the level of diffusion.

5. The effect of chaos and molecular diffusion in filter feeding

In the previous section we studied the effects of chaotic advection on filter feeding, using the model of the blinking stokeslet. In general molecular diffusion can play an important rôle in determining the transport of nutrients through such a flow. In order to give some conclusive and quantitative results on the effect of chaos on filter feeding, and answer the question of whether there are any particular switching protocols that can lead to optimum 'feeding' we will assume that the nutrient undergoes the effects of advection and molecular diffusion. In such a case the concentration of the nutrient $n(x, y, t)$ (as a function of space and time) will satisfy the following diffusion–advection

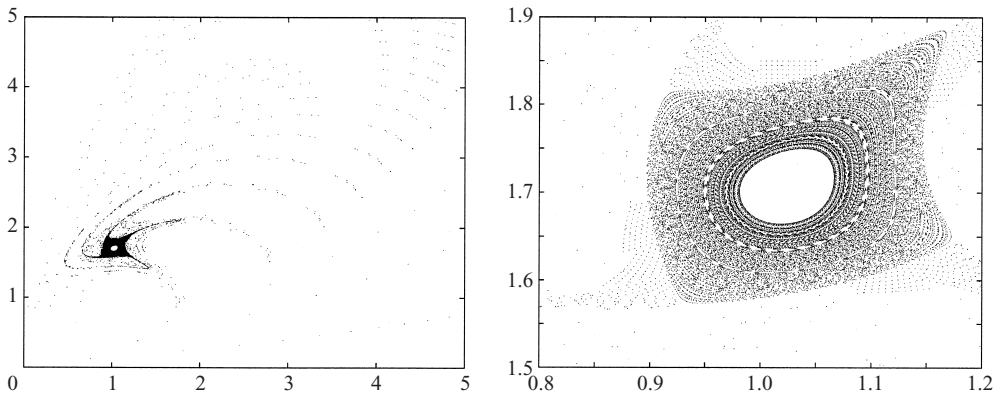

FIGURE 13. Poincaré section shown for $\alpha^{(1\pm\epsilon)} = 5/2$, with an enlargement of the area close to the fixed point.

equation

$$\frac{\partial n}{\partial t} + \nabla \cdot (\boldsymbol{u} n) = D\nabla^2 n \tag{5.1}$$

where $\boldsymbol{u} = \boldsymbol{u}(x, y, t)$ is the velocity field generated by the blinking stokeslet if the nutrient is assumed to undergo no inertial effects (its density is the same as the density of the ambient fluid) or given by the model in § 3 in the case where density differences are important. In the first case the velocity field experienced by the nutrient particles is divergence free whereas in the second case the nutrient particles experience a compressible velocity field and this is likely to have important effects on transport.

In the case of particles with inertia the diffusion–advection equation, (5.1), will still be a valid model but the advecting velocity field will be modified. We will assume that the particles are subject to a stochastic force $\boldsymbol{F}_s$ which gives rise to a diffusive phenomenon. In that case then the equation defining the rate of change of the particle velocity, (3.1), will need to be modified by the addition of the force $\boldsymbol{F}_s$. In the case where the ratio of particle and fluid density is almost unity, an asymptotic analysis analogous to that of Druzhinin & Ostrovsky (1994) shows that the local velocity field the particles will experience will be of the form

$$\boldsymbol{v} = \boldsymbol{u} + \gamma \frac{\mathrm{D}\boldsymbol{u}}{\mathrm{D}t} + \alpha \boldsymbol{F}_s,$$

where α is a numerical factor associated with the strength of the stochastic force.

The particle paths will then be given by the solution of the stochastic differential equation (SDE)

$$\dot{\boldsymbol{x}} = \boldsymbol{v},$$

which under the assumption that $\boldsymbol{F}_s$ is the 'derivative' of the Wiener process (defined in a proper generalized sense) is equivalent to an advection–diffusion equation with a modified advecting velocity field.

In the case where the parameters are such that this reduction is not permitted then we need to work with the original SDE containing information on both the momenta and the position of the particles. This SDE is equivalent to a Fokker–Planck equation with diffusive terms in the momenta. Since the information on the momenta is 'redundant', we can average the particle probability distribution over momenta. This averaging procedure will result in an effective advection–diffusion

equation in position variables only, with some effective advecting field and some effective diffusivity tensor. This approach is very common in rheology studies or in cases where the tracer has extra degrees of freedom (for an example of an application of such idea in a problem of gyrotaxis see Pedley & Kessler 1990).

A quantity of biological interest is the efficiency of filter feeding under the effects of chaos. We consider the feeding current to the micro-organism, averaged over its length and over a period of the switching protocol:

$$F_c = \frac{1}{T}\int_{nT}^{(n+1)T}\int_0^1 \left.\frac{\partial n(x,y,t)}{\partial x}\right|_{x=0} \mathrm{d}y\,\mathrm{d}t, \tag{5.2}$$

where in normalized coordinates the micro-organism is taken to extend from $y = 0$ to $y = 1$. The feeding current will be a function of D, n and the period (and functional form) of the switching protocol. We expect that chaos will lead to an enhancement of this quantity. In the case where T is chosen in such a way that the motion of the nutrient is regular and the nutrient is bound to stay on the contours of the stream function, one expects that the only feeding current will be that due to molecular diffusion. The effect of chaos will be to give an additional feeding current to that of diffusion and so will enhance the feeding capacity of the micro-organism.

In order to check this intuitive notion in a quantitative manner we solve the diffusion–advection equation (5.1) for an initial condition localized above the centre of the vortex created by the stokeslets. The equation is solved using finite-differences and an ADI scheme. Using this numerical solution we calculate the feeding current (5.2) and plot it as a function of n (number of blinks of the pairs of stokeslets) for different values of molecular diffusion and T. The optimal switching protocol would be chosen as the one that gives a maximum of the feeding current for the smallest possible value of n (since the medium is very viscous, it is energetically very expensive for the micro-organism to beat its flagella for a large number of times). The nutrient is initially placed above the core of the eddy and the level of diffusion is taken to be that corresponding to the level of noise used in the stochastic calculations. We have not embarked on an extensive optimization of the feeding since the number of arbitrary parameters is large. This fact, coupled to the lack of experimental data, means that our results are unlikely to provide any more information than that the feeding currents are enhanced as $\alpha^{(1\pm\epsilon)}$ increases, almost irrespective of the initial nutrient distribution. We now go on to discuss a method whereby the generic level of feeding is determined.

An alternative approach to solving this partial differential equation would be to introduce some white noise terms in the maps we have proposed. The maps will then become

$$\boldsymbol{r}_{n+1} = M(\boldsymbol{r}_n) + \xi_n,$$

where the ξ_n are identically distributed Gaussian variables with standard deviation equal to D. The feeding current can then be calculated as the average of the feeding current for a number of realizations of the white noise terms. This approach is equivalent to the partial differential equation approach and is expected to give similar results if the averaging is performed over a large number of realizations of the noise terms, Oksendal (1985).

This can be seen by the application of the celebrated Feynman–Kac formula which connects the solution of the parabolic PDE

$$\frac{\partial P}{\partial t} = \boldsymbol{u}\cdot\nabla P + D\nabla^2 P, \qquad P(\boldsymbol{r},0) = P_0(\boldsymbol{r}),$$

as the expectation

$$P(\boldsymbol{r}, t) = E_{\boldsymbol{r}} P_0(\boldsymbol{r}(t)),$$

where $\boldsymbol{r}(t)$ is the solution of the SDE

$$\dot{\boldsymbol{r}}(t) = \boldsymbol{u}(\boldsymbol{r}(t)) + \sqrt{2D}\dot{\boldsymbol{W}}, \tag{5.3}$$

where $\boldsymbol{W}$ is the Wiener process, Oksendal (1985). The term $E_{\boldsymbol{r}}$ means that the averaging is performed over all paths of the stochastic process (5.3) satisfying $\boldsymbol{r}(0) = \boldsymbol{r}$. In the limit $D \to 0$ this solution reduces to the solution of a first-order PDE using the method of characteristics. A straightforward time discretization will give us the proposed map.

Because of the complexity of the flow field an analytical approach to the problem is impossible. One possibility for obtaining (semi-)analytical results would be to study the case where diffusion is dominant and treat the advection term as a perturbation to the diffusion operator. This approach may be relevant near stagnation points of the flow.

Using this stochastically perturbed map, we can measure the effects of chaos on the phenomenon of filter feeding, by performing the following numerical experiment. We start a distribution of initial conditions that represent the nutrient in a part of the phase space which has no common intersection with a subset of phase space near the micro-organism which we associate with the mouth region. We then assume there is an absorbing boundary condition on the boundary of the mouth region and we run each initial condition until it enters the mouth region. When an initial condition enters this region, it is removed from the initial ensemble of particles. We then calculate the fraction of initial conditions that have reached the mouth area and have been absorbed as a function of time. This quantity, which is related to the feeding current in the vicinity of the micro-organism, gives us the probability that nutrient reaches the mouth region. Since, without the effects of diffusion and advection the nutrient would never reach the mouth region, given that it has started away from it, this quantity gives us the effect of diffusion and advection on the feeding of the micro-organism. Because of the lack of sufficient physiological data, we were rather arbitrary in assigning the 'area' of the mouth region. Also, the absorbing boundary condition we introduced is biologically relevant, since it is commonly believed that the flow is responsible for moving the nutrient to a neighbourhood of the mouth and then other processes take over to bring the nutrient into the mouth, for instance chemical gradients, phagocytosis or macropinocytosis.

In figure 14(*a*) we show the fraction of nutrient that reached the mouth region in up to 600 iterations in the case where molecular diffusion is absent. This fraction is calculated for different values of the parameter $\alpha^{(1\pm\epsilon)}$ which as we saw is related to the degree of chaos in the streamline dynamics. As we expect intuitively this fraction increases significantly as the parameter $\alpha^{(1\pm\epsilon)}$ increases, thus quantifying the statement that the breakup of invariant curves in the dynamics is going to lead to an increase of the current towards the micro-organism. In figure 14(*b*) the same quantity is calculated when the effect of molecular noise is present. It is seen that the effect of molecular noise is to smooth the results (especially in the small $\alpha^{(1\pm\epsilon)}$ limit). The same qualitative behaviour is present, i.e. the probability of entry into the mouth region is greater the larger $\alpha^{(1\pm\epsilon)}$ is, as happened in the deterministic case. It is worth noting that for small values of n both in the deterministic and the molecular diffusion case the graphs are not strictly ordered. This is because the choice of initial conditions was done on a random grid and this behaviour is due to short-time transients, i.e. initial conditions

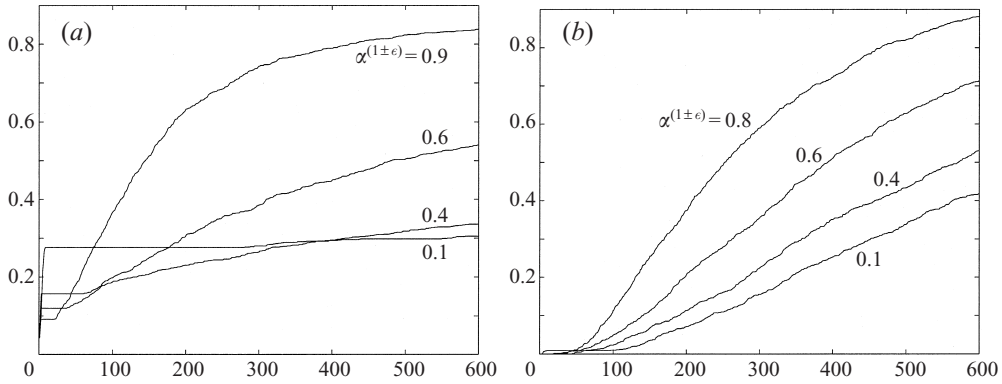

FIGURE 14. Probability of food particles entering the mouth region against number of periods of the map. (*a*) without white noise, (*b*) with white noise.

that were transported by the flow into the mouth region simply because they started very close to it. The strict ordering of the graphs starts after a critical time, when all the transients have died out. In both the deterministic and the molecular noise case the mouth region was taken to be the interval $[-0.3, 0.3] \times [0.5, 1.5]$, the initial condition consists of an ensemble of 1000 particles and the noise amplitude was 0.03.

6. Conclusions

This work was initially motivated by a study of the feeding currents around a sessile micro-organism attached to a rigid wall. The various organelles on the micro-organisms effectively exert a force either towards or away from the boundary. The flow field associated with such a motion leads to a single toroidal eddy. However these organisms often regularly alter the length of the stalk attached to the boundary leading to a similar toroidal eddy but displaced a vertical distance from the earlier one. Thus, because we have a low-Reynolds-number flow with no inertia, a food particle can 'hop' from one streamline to another one, the basis for the chaotic behaviour analysed in this paper. Flow at low Reynolds numbers in confined geometries is now known to be extremely complicated so that the relatively simple study developed in this paper is likely to have qualitatively similar implications for other flows where the eddy structure can be modified; examples include bolus flow between red blood cells, airflow in alveoli and fine-scale micro-turbulent mixing processes. The analysis within the paper reveals the rich structure of the mixing process and the effects that inertia and Brownian motion may have on the mixing patterns.

The measures we have exploited here, especially Lyapunov exponents (and inherently the Jacobian), are concerned with the local stretching of fluid elements, which is applicable to the mixing of nutrients and their transport to mouth regions. We have demonstrated that the presence of chaos will enhance the likelihood of feeding, with and without molecular diffusion (modelled via the inclusion of white noise).

By the use of a map we have been able to study the inherent chaotic structures of this problem and provide a direct link between the level of chaos and the possibility for filter feeding. To repeat an earlier sentiment, the occurrence of varying eddy structures within Stokes flow has been demonstrated to be central to the enhancement of mixing and transport processes. The increase of the maximum local Lyapunov exponent and the structures depicted in figure 9 underline this conclusion.

Appendix. Derivation of the two-dimensional area-preserving map

We shall now comment upon the construction of a suitable map. We assume that we are considering an incompressible fluid and as such the particle paths are determined by the solution of the equations

$$\dot{x} = \frac{\partial \psi}{\partial y} \quad \text{and} \quad \dot{y} = -\frac{\partial \psi}{\partial x},$$

where $\psi = \psi(x, y, t)$. These expressions can be integrated to give

$$x(t) = x(0) + \int_{\tau=0}^{t} \frac{\partial \psi}{\partial y}(x, y, \tau)\, \mathrm{d}\tau \quad y(t) = y(0) - \int_{\tau=0}^{t} \frac{\partial \psi}{\partial x}(x, y, \tau)\, \mathrm{d}\tau.$$

We now consider an inertia-free flow such that $\psi(x, y, t) = \bar{\psi}(x, y)\delta(t - T/2)$, with $(x(0), y(0)) = (x_0, y_0)$ and $(x(T), y(T)) = (x_1, y_1)$. In due course we will generalize this to a periodic chain of pulses. For $0 < t < T/2$ there is no motion so that $(x(t), y(t)) = (x_0, y_0)$ during this interval, and similarly $(x(t), y(t)) = (x_1, y_1)$ for $t > T/2$. Hence we have

$$x_1 = x_0 + \lim_{\epsilon \to 0} \int_{\tau=T/2-\epsilon}^{\tau=T/2+\epsilon} \frac{\partial \bar{\psi}}{\partial y}(x, y)\delta(\tau - T/2)\, \mathrm{d}\tau \quad \text{and}$$

$$y_1 = y_0 - \lim_{\epsilon \to 0} \int_{\tau=T/2-\epsilon}^{\tau=T/2+\epsilon} \frac{\partial \bar{\psi}}{\partial x}(x, y)\delta(\tau - T/2)\, \mathrm{d}\tau.$$

Initially it would seem sensible to 'evaluate' the velocity components at (x_0, y_0), yielding the explicit map

$$x_1 = x_0 + \frac{\partial \bar{\psi}}{\partial y}(x_0, y_0) \quad \text{and} \quad y_1 = y_0 - \frac{\partial \bar{\psi}}{\partial x}(x_0, y_0).$$

This map is easy to use and is computationally inexpensive; however it is not area preserving. This means that the incompressibility of the flow has been lost. It is possible to rectify this situation by evaluating the velocities at (x_0, y_1) or (x_1, y_0) (the corresponding maps are referred to herein as implicit in y and implicit in x respectively). In some problems one is able to decide which to use via a physical argument. In the problem considered here this is not the case, and consequently the choice is arbitrary. The resulting maps are both implicit and relatively easy to work with. In the former case (implicit in y) the second equation needs to be solved for y_1 (which was done using the MATLAB routine fzero) and then that value can be substituted into the other equation to give x_1. A similar technique is used for the map which is implicit in x.

In order to rectify the uncertainty, we use the Poincaré map for which the velocity components are evaluated at the midpoint of the interval. The resulting map is

$$x_1 = x_0 + \frac{\partial \bar{\psi}}{\partial y}\left(\frac{x_0 + x_1}{2}, \frac{y_0 + y_1}{2}\right) \quad \text{and} \quad y_1 = y_0 - \frac{\partial \bar{\psi}}{\partial x}\left(\frac{x_0 + x_1}{2}, \frac{y_0 + y_1}{2}\right).$$

This has an intrinsic symmetry both in space and time, and it is also area preserving. This scheme is essentially a midpoint integration rule. The rationale behind this choice is that the δ-functions introduce a discontinuity at which we assume the value of the function is evaluated at the mean of the left and right limits.

The Jacobian of this map is

$$\boldsymbol{J} = \begin{pmatrix} \dfrac{\Delta + 4(1+\bar{\psi}_{xy})}{4-\Delta} & \dfrac{4\bar{\psi}_{xx}}{\Delta - 4} \\ -\dfrac{4\bar{\psi}_{yy}}{4-\Delta} & \dfrac{\Delta + 4(1-\bar{\psi}_{xy})}{\Delta - 4} \end{pmatrix}, \tag{A 1}$$

where $\Delta = \bar{\psi}_{xy}^2 - \bar{\psi}_{xx}\bar{\psi}_{yy}$, which is the Hessian of the map. In the above matrix all the quantities are evaluated at the midpoint $\big((x_0+x_1)/2, (y_0+y_1)/2\big)$. The trace of this matrix is

$$\mathrm{Tr}(\boldsymbol{J}) = 2\frac{\Delta + 4}{4-\Delta}.$$

This means that the condition for a fixed point to be elliptic is that the Hessian is negative (cf. the Hénon index). In order to solve the implicit equations for (x_1, y_1) we use a two-dimensional Newton–Raphson scheme. We introduce the two functions

$$f(x_1, y_1) = x_1 - x_0 - \frac{\partial\bar{\psi}}{\partial y}\left(\frac{x_0+x_1}{2}, \frac{y_0+y_1}{2}\right) \quad \text{and}$$

$$g(x_1, y_1) = y_1 - y_0 + \frac{\partial\bar{\psi}}{\partial x}\left(\frac{x_0+x_1}{2}, \frac{y_0+y_1}{2}\right),$$

and it is relatively simple to construct the partial derivatives of f and g with respect to x_1 and y_1. In order to obtain an initial guess for (x_1, y_1) the explicit scheme was used as a predictor, and then this guess was refined by using a fixed-point iteration as a corrector (notice that this only works when both eigenvalues of the matrix $\partial(f,g)/\partial(x_1, y_1)$ are less than unity. The necessary, but not sufficient condition, is that the modulus of the determinant must be less than unity). For problems in which the predictor/corrector technique was not applicable, we exploited the explicit map with a large number of steps with the requisite choice of stokeslet parameter (that is N steps with a stokeslet characterized by $\alpha_s^{(1\pm\epsilon)} = \alpha^{(1\pm\epsilon)}/N$).

These maps are easily extended to the current system where for the first stokeslet we replace (x_0, y_0) by (x_n, y_n) and (x_1, y_1) by $(x_{n+1/2}, y_{n+1/2})$ and then by $(x_{n+1/2}, y_{n+1/2})$ and (x_{n+1}, y_{n+1}) respectively for the second one. In this case the corresponding stream function is used for $\bar{\psi}(x, y)$, that is $\psi^{(1\pm\epsilon)}(x, y)$ defined in (2.2).

REFERENCES

Antonsen T. M. & Ott E. 1991 Multifractal power spectra of passive scalars convected by chaotic fluid flows. *Phys. Rev.* A **44**, 851–857.

Aref, H. 1984 Stirring by chaotic advection. *J. Fluid Mech.* **143**, 1–21.

Blake, J. R. & Otto, S. R. 1996 Ciliary propulsion, chaotic filtration and a 'blinking' stokeslet. *J. Engng Maths* **30**, 151–168.

Blake, J. R., Otto, S. R. & Blake, D. A. 1998 Filter feeding, chaotic filtration and a blinking stokeslet. *Theor. Comput. Fluid Dyn.* **10**, 23–36.

Bohr, T. & Rand, D. 1987 The entropy function for characteristic exponents. *Physica* D **25**, 387–398.

Druzhinin, O. A. & Ostrovsky, L. A. 1994 The influence of Basset force on particle dynamics in 2-dimensional flows. *Physica* D **76**, 34–43.

Eckhardt, B. & Yao, D. 1993 Local Lyapunov exponents in chaotic systems. *Physica* D **65**, 100–108.

Gaspard, P. & Nicolis, G. 1990 Transport properties, Lyapunov exponents, and entropy per unit time. *Phys. Rev. Lett.* **65**, 1693–1696.

Hackborn, W. W., Ulucakli, M. E. & Yuster, T. 1997 A theoretical and experimental study of hyperbolic and degenerate mixing regions in a chaotic Stokes flow. *J. Fluid Mech.* **346**, 23–48.

Hénon, M. 1969 Numerical study of quadratic area-preserving mappings *Q. Appl. Maths* **27**, 291–312.

Higdon, J. J. L. 1979 The generation of feeding currents by flagellar motions. *J. Fluid Mech.* **94**, 305–330.

Jana, S. C., Metcalfe, G. & Ottino, J. M. 1994 Experimental and computational studies of mixing in complex Stokes flows: the vortex mixing flow and multicellular flows. *J. Fluid Mech.* **269**, 199–246.

Khakhar, D. V., Rising, H. & Ottino, J. M. 1986 An analysis of chaotic mixing in two chaotic flows. *J. Fluid Mech.* **172**, 419–451.

Lochak, P. & Meunier, P. *Multiphase Averaging in Classical and Quantum Systems.* Springer.

Lorentz, H. A. 1896 Eene algemeene stelling omtrent de beweging eener vloeistof met wrijving en eenige daaruit afgeleide gevolgen. *Zittingsverslag Koninkl. Akad. van Wetensch. Amsterdam* **5**, 168–175.

Maxey, M. R. & Riley, J. J. 1983 Equation of motion for small rigid sphere in a nonuniform flow. *Phys. Fluids* **26**, 883–889.

Maxey, M. R. 1990 On the advection of spherical and nonspherical particles in a nonuniform flow. *Phil. Trans. R. Soc. Lond.* A **333**, 289–307.

Maxey, M. R., Patel, B. K., Chang, E. J. & Wang, L. P. 1997 Simulations of dispersed turbulent multiphase flow. *Fluid Dyn. Res.* **20**, 143–156.

Oksental 1985 *Stochastic Differential Equations: an Introduction with Applications.* Springer.

Omurtag, A. C., Dutta, P. & Chevray, R. 1996 Attractors of finite-sized particles: An application to enhanced separation. *Phys. Fluids* **8**, 3213–3214.

Ottino, J. M. 1989 *The Kinematics of Mixing: Stretching, Chaos and Transport*. Cambridge University Press.

Pedley, T. J. & Kessler, J. O. 1990 A new continuous model for suspensions of gyrotactic micro-organisms. *J. Fluid Mech.* **212**, 155–182.

Pettitt, M. E. 2000 Prey capture and ingestion in choanoflagellates. PhD thesis, The University of Birmingham.

Sleigh, M. A. 1973 *The Biology of Protozoa.* Edward Arnold.

Tang, X. C. & Boozer, A. H. 1996 Finite time Lyapunov exponent and advection-diffusion equation. *Physica* D **95**, 283–305.

Varosi F., Antonsen T. M. & Ott E. 1991 The spectrum of fractal dimensions of passively convected scalar gradients in chaotic fluid flows. *Phys. Fluids* A **3**, 1017–1028.

Wiggins, S. 1992 *Transport in chaotic dynamical systems.* Springer.

Yannacopoulos, A. N. & Rowlands, G. 1997 Local transport coefficients for chaotic systems. *J. Phys.* A: *Math. Gen.* **30**, 1503–1525.

Yannacopoulos, A. N., Rowlands, G. & King, G. P. 1999 Motion of particles with inertia in vortical flows under the effects of molecular diffusion: analytic results in the small inertia limit. Preprint.